This article was downloaded by: [Renmin University of China]
On: 13 October 2013, At: 11:06
Publisher: Taylor & Francis
Informa Ltd Registered in England and Wales Registered Number: 1072954 Registered office: Mortimer House, 37-41 Mortimer Street, London W1T 3JH, UK

Molecular Crystals and Liquid Crystals
Publication details, including instructions for authors and subscription information:
http://www.tandfonline.com/loi/gmcl20

Frequency-Controlled Routing of Self-Confined Beams in Nematic Liquid Crystals

Armando Piccardi [a], Alessandro Alberucci [a], Oleksandr Buchnev [b], Malgosia Kaczmarek [b], Iam-Choon Khoo [c] & Gaetano Assanto [a]

[a] NooEL (NonLinear Optics and Optoelectronics Laboratory), University of Roma Tre, Rome, Italy

[b] School of Physics and Astronomy, University of Southampton, Southampton, United Kingdom

[c] Department of Electrical Engineering, Pennsylvania State University, University Park, PA, USA

Published online: 02 Apr 2013.

To cite this article: Armando Piccardi, Alessandro Alberucci, Oleksandr Buchnev, Malgosia Kaczmarek, Iam-Choon Khoo & Gaetano Assanto (2013) Frequency-Controlled Routing of Self-Confined Beams in Nematic Liquid Crystals, Molecular Crystals and Liquid Crystals, 573:1, 26-33, DOI: 10.1080/15421406.2013.763334

To link to this article: http://dx.doi.org/10.1080/15421406.2013.763334

PLEASE SCROLL DOWN FOR ARTICLE

Taylor & Francis makes every effort to ensure the accuracy of all the information (the "Content") contained in the publications on our platform. However, Taylor & Francis, our agents, and our licensors make no representations or warranties whatsoever as to the accuracy, completeness, or suitability for any purpose of the Content. Any opinions and views expressed in this publication are the opinions and views of the authors, and are not the views of or endorsed by Taylor & Francis. The accuracy of the Content should not be relied upon and should be independently verified with primary sources of information. Taylor and Francis shall not be liable for any losses, actions, claims, proceedings, demands, costs, expenses, damages, and other liabilities whatsoever or howsoever caused arising directly or indirectly in connection with, in relation to or arising out of the use of the Content.

This article may be used for research, teaching, and private study purposes. Any substantial or systematic reproduction, redistribution, reselling, loan, sub-licensing, systematic supply, or distribution in any form to anyone is expressly forbidden. Terms &

Conditions of access and use can be found at http://www.tandfonline.com/page/terms-and-conditions

Downloaded by [Renmin University of China] at 11:06 13 October 2013

Mol. Cryst. Liq. Cryst., Vol. 573: pp. 26–33, 2013
Copyright © Taylor & Francis Group, LLC
ISSN: 1542-1406 print/1563-5287 online
DOI: 10.1080/15421406.2013.763334

Taylor & Francis
Taylor & Francis Group

Frequency-Controlled Routing of Self-Confined Beams in Nematic Liquid Crystals

ARMANDO PICCARDI,[1,*] ALESSANDRO ALBERUCCI,[1] OLEKSANDR BUCHNEV,[2] MALGOSIA KACZMAREK,[2] IAM-CHOON KHOO,[3] AND GAETANO ASSANTO[1]

[1]NooEL (NonLinear Optics and Optoelectronics Laboratory), University of Roma Tre, Rome, Italy
[2]School of Physics and Astronomy, University of Southampton, Southampton, United Kingdom
[3]Department of Electrical Engineering, Pennsylvania State University, University Park, PA, USA

We demonstrate the electro-optic control of self-confined beams via frequency modulation in dual-frequency nematic liquid crystals. Proper design of comb electrodes in a planar cell allows the maximization of the overall steering angle when only walk-off variations are used. A span angle as large as two times the maximum walk-off angle is achieved.

Keywords nonlinear optics; Dual Frequency Liquid Crystals; reorientational response; spatial solitons routing; spatial solitons

OCIS codes (160.3710) Liquid crystals; (190.0190) Nonlinear optics; (190.5940) Self-action effects; (190.6135) Spatial solitons

Downloaded by [Renmin University of China] at 11:06 13 October 2013

1. Introduction

Nematic liquid crystals (NLCs) are extremely versatile media allowing easy tuning of their physical properties through the application of electric/optical fields [1]; the NLCs' high polarizability stems from the rotation of their strongly anisotropic molecules in response to external electromagnetic fields regardless of the frequency. When shined with light, NLC behave like uniaxial media with the optic axis parallel to the molecular director $\boldsymbol{n}$, i.e., the average direction of the molecular long axis alignment [2], and show a large optical birefringence $\Delta n = n_{||} - n_{\perp}$, $n_{||}$ and $n_{\perp}$ being the refractive indices associated to the direction parallel and perpendicular to the director. The high birefringence, jointly with the ease in director rotation, provides huge nonlinear coefficients via the so-called reorientational nonlinearity, making NLCs ideal candidates for the investigation of nonlinear optical effects [3]. In particular, when an extraordinary polarized finite-size beam propagates inside an NLC layer, an inhomogeneous distribution of the molecular director is induced due to

*Address correspondence to Armando Piccardi, NooEL (NonLinear Optics and Optoelectronics Laboratory), University of Roma Tre, Via della Vasca Navale 84, Rome, Italy. E-mail: apiccardi@uniroma3.it

Downloaded by [Renmin University of China] at 11:06 13 October 2013

the optical reorientation: if power is high enough (typically few milliwatts), a bell-shaped refractive index profile able to trap the beam itself is generated. The power threshold is related with the interplay among the self-focusing effect and the energy spreading due to diffraction: when the two effects exactly balance each other, a spatial soliton propagates, i.e., a nonlinear wave preserving its transversal profile while propagating [4,5]. Due to strong elastic forces between NLC molecules, the optical director perturbation is much larger than the light intensity profile; thus, the reorientational nonlinearity shows a large nonlocal character. Nonlocality stabilizes $(2+1)D$ spatial solitons otherwise unstable in local Kerr media [6,7]. A lot of attention has been devoted to the study of optical spatial solitons, both for the universality character of their properties [8] and for the potential applications in modern systems of optical processing due to their character of self-induced waveguides [9]. NLCs offer unique properties with respect to other nonlinear materials where spatial solitons are observed [10–13]: low powers are needed for their excitation and a wide tunability of their properties is easily accessible [14].

During the last years, spatial solitons in NLCs, namely nematicons [15], have been demonstrated to be generated and routed in a plenty of configurations, based upon the control of the wave/Poynting vector via gradient index and/or of the walk-off angle. Index gradients are typically given by electrically or optically induced inhomogeneities in the director distribution [16–19]. Nematicon routing based only upon walk-off changes related with director rotation across all the NCL layer has been demonstrated as well [20]. Moreover, self-steering has been achieved in the nonlinear nonperturbative regime and employing guest–host interactions in a dye-doped NLC [21,22].

With reference to the electric fields, most of NLC have a flat dielectric response from low frequency to the megahertz region, with a positive dielectric anisotropy $\Delta\varepsilon = \varepsilon_{||} - \varepsilon_{\perp}$. There exists a class of liquid crystalline materials, namely dual-frequency NLC (DFNLC) [23], exhibiting a strongly dispersive susceptibility parallel to $\boldsymbol{n}$ at extremely low frequency, due to the presence of an orientational contribution featuring a single pole response in the frequency domain [23–26]. Given that it is $\Delta\varepsilon > 0$ around the frequency $f = 0$ and that the perpendicular susceptibility $\varepsilon_{\perp}$ remains nearly constant versus f, the dielectric anisotropy changes dramatically and even changes sign around a crossover frequency f_c, the latter corresponding to a null dielectric anisotropy. As a result, the electric torque $\mathbf{M}_{\mathrm{LF}} \propto \Delta\varepsilon_{\mathrm{LF}}(f)\,|E_{\mathrm{LF}}|^2$ (E_{LF} stands for the low-frequency electric field) acts in different directions whether the frequency of the applied field is below or above the crossover value. These properties have been employed to improve the recovery time of NLC-based optical devices, and to implement filters, modulators, or displays [27–29].

In this work, we employ the peculiar electro-optic response of a DFNLC to control the nematicon trajectories, varying both the frequency and the amplitude of the applied bias. In the used scheme, nematicon routing is related only with walk-off variations, i.e., rotation of the director is uniform inside the sample. We use a suitable designed sample to maximize the Poynting vector steering under these conditions, reaching an angular deflection of about 13° (twice the maximum walk-off angle for the provided NLC mixture), varying the frequency of the applied electric field from 1 to 100 kHz for a fixed amplitude.

2. Theoretical Approach and Sample Design

The sample used is composed by two glass slides separated by $h = 100\ \mu$m with the use of Mylar spacers. The inner surface of each slab is mechanically treated in order to favor the molecular alignment along the z-direction, with reference to Fig. 1. To obtain a

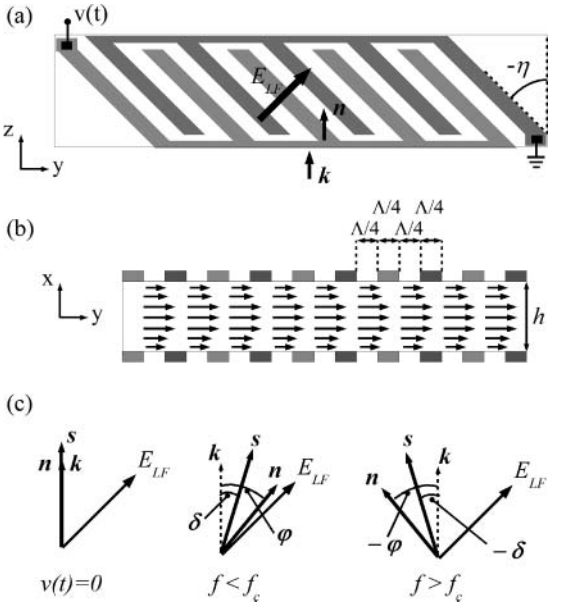

Figure 1. Sample description. (a) Top view of the cell, with the sketch of the patterned electrodes. (b) Front view of the cell, with the indication of the director distribution when a voltage is applied. (c) Pictorial view of the working principle: when a voltage is applied, the director rotates depending on the electric field, causing a rotation of the optic axis and thus of the Poynting vector. This rotation is positive or negative when $f < f_c$ or $f > f_c$, respectively.

planar electric reorientation, patterned electrodes are used [30], as sketched in Fig. 1(a) and (b): two interdigitated comb-like structures are created, the teeth orientated at $\eta = 45^\circ$ with respect to the z-axis. The width of each tooth is $\Lambda/4 = 15$ μm, each comb having a period of $\Lambda = 60$ μm. The sample is filled by capillarity with the MLC-2048 DFLC [29–31].

When a voltage is applied between the two electrodes/combs, an electric field with a period of 60 μm is established nearby the glass–NLC interfaces; for the chosen geometrical parameters, the vertical (x-) component of E_{LF} is negligible for moderate values of the applied voltage; thus, the relevant component of the field is directed perpendicularly to the teeth, at an angle η with respect to the initial molecular director. Electric reorientation can be considered to occur only in the nearby of the surfaces, while elastic forces ensure a homogeneous planar rotation in the bulk: in fact, the nonlocality is dictated by the cell thickness h [32] and thus is much larger than the field period [33]. The director rotation φ, the angle between $\boldsymbol{n}$ and the z-axis, occurs in the y–z plane, toward negative or positive values depending on the field frequency f, with the available electrically driven reorientation spanning in the interval $-45^\circ < \varphi < 45^\circ$, depending on both voltage amplitude and frequency. To mathematically describe the director reorientation in the absence of light, we employ the reorientational equation:

$$\frac{\partial^2 \varphi}{\partial x^2} + \frac{\partial^2 \varphi}{\partial \xi^2} + \frac{\varepsilon_0 \Delta \varepsilon_{\mathrm{LF}}(f)}{2K} \sin\left[2(\eta - \varphi)\right] |E_{\mathrm{LF}}|^2 = 0, \tag{1}$$

where we adopted a reference system $x\xi\zeta$ rotated by η with respect to the axis x, with ε_0 being the vacuum dielectric permittivity and K the scalar Frank's constant [2,3].

Downloaded by [Renmin University of China] at 11:06 13 October 2013

Downloaded by [Renmin University of China] at 11:06 13 October 2013

Regarding the light evolution, we assume that the director lies on the plane y–z and is uniformly distributed, forming an angle φ_0 with the axis z; φ_0 is the solution of Equation (1) taken in $x = h/2$, i.e., in the cell mid-plane. Thus, for a beam launched with wave vector along the z axis and positioned in the sample mid-plane, we can model the nonlinear optical propagation using a nonlinear Schrödinger equation in (1+1)D [33]:

$$2ik_0n_0\left\{\frac{\partial A}{\partial z}+\tan\left[\delta\left(\varphi_0\right)\right]\frac{\partial A}{\partial y}\right\}+D_y\frac{\partial^2 A}{\partial y^2}+k_0^2\Delta n_{\mathrm{e}}^2\left(\varphi_0,\theta\right)A=0, \tag{2}$$

where k_0 and n_0 are the vacuum wave vector and the averaged refractive index, respectively, A is the envelope of the optical field, δ is the walk-off angle, Δn_e^2 is the nonlinear index well responsible for photons self-trapping, and D_y is the diffraction constant along the y-direction. The dependence on the reorientation angle φ_0 has been explicitly written for δ and Δn_{e}^2; noteworthy, the confining term depends also on the nonlinear perturbation θ on the director distribution. The walk-off angle is defined as

$$\delta\left(\varphi_0\right)=\arctan\left[\frac{\varepsilon_a\sin\left(2\varphi_0\right)}{\varepsilon_a+2\varepsilon_\perp+\varepsilon_a\cos\left(2\varphi_0\right)}\right], \tag{3}$$

with $\varepsilon_a=\varepsilon_{||}-\varepsilon_\perp$ the optical anisotropy. Angle δ given by (3) defines the angle formed by the Poynting vector with the wave vector, and, given the birefringence of the employed DFNLC ($\Delta n\approx 0.2$) ranges between -7° and 7° (see Fig. 1(c)). The dependence of Δn_{e}^2 on to φ_0 can be addressed introducing an equivalent nonlocal Kerr coefficient [33]:

$$n_2=\frac{\varepsilon_0\varepsilon_{\mathrm{a}}}{2K}\sin\left[2\left(\varphi_0-\delta\right)\right]n_{\mathrm{e}}^2\left(\varphi_0\right)\tan\delta\left(\varphi_0\right). \tag{4}$$

Equations (3) and (4) show how both the trajectory and the width of light beams depend, through Equation (1), on the dielectric anisotropy $\Delta\varepsilon_{\mathrm{LF}}$ and, thus, on the frequency of the applied field E_{LF}.

3. Experiments

We coupled a y-polarized infrared beam, $\lambda = 1064$ nm, into the cell described in Fig. 1, with the wave vector $\mathbf{k}$ parallel to the z axis and an initial width of $w_0 = 3$ mm. The power is $P =$ 15 mW, enough to observe self-confinement in almost all the amplitude/frequency range, without suffering detrimental effects due to temporal instabilities and thermal heating [21]. The observation of the beam evolution on the plane y–z is carried out with a microscope camera collecting the light scattered out of the propagation plane. A voltage in the form $\mathrm{v}(t)=\sqrt{2}V\sin\left(2\pi ft\right)$ is applied to the sample. In the unbiased case, the beam propagates along z ($\varphi_0 = 0$ in Eq. (3)) and diffracts at any power, as the optical reorientation is inhibited by the Fréedericksz threshold [3].

We performed a first sample characterization by observing the optical propagation at different voltages for two different frequencies (one lower and one higher than f_{c}), measuring how the walk-off changes with the applied bias [20]. Results are shown in Fig. 2. At the lowest frequency $f = 1$ kHz (Fig. 2(a)–(c)), walk-off increases as the amplitude is raised from $V = 0$ V up to $V = 6$ V, where it reaches the maximum value of $\delta = 6.5^\circ$ (see Fig. 2(c)), coherently with the DFNLC birefringence. Additional increases in the voltage amplitude did not cause any further beam motion: we reached the saturation of the reorientational response at $\varphi_0 = \eta = 45^\circ$, i.e. $\boldsymbol{n}\|\boldsymbol{E}_{\mathrm{LF}}$. At $f = 100$ kHz (Fig. 2(d)–(f)),

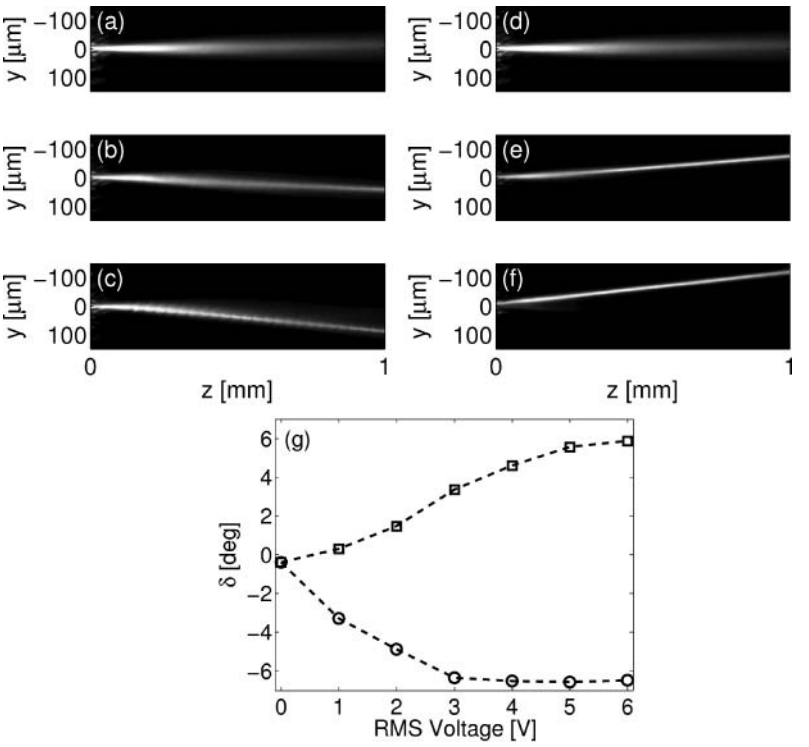

Figure 2. Acquired pictures for voltage $V = 0$ V (a, d), 3 V (b, e), 6 V (c, f) and frequency $f =$ 1 kHz (a–c) and 100 (d–f) kHz. (g) Curves of the measured walk-off for $f = 1$ kHz (squares) and 100 (circles) kHz vs. voltage. The dashed lines are guidelines for eyes.

Downloaded by [Renmin University of China] at 11:06 13 October 2013

the dielectric anisotropy is negative; thus, the beam steers toward the opposite direction up to $\delta = -6.5^\circ$ (see Fig. 2(f)) in correspondence to $\varphi_0 = -45^\circ$, and for the same amplitude range as in the previous case, with a nearly symmetric curve (Fig. 2(g)).

To investigate the performances of this sample as a frequency-controlled router, we chose the saturation value $V = 6$ V and varied the frequency. Starting from $f = 1$ kHz (Fig. 3(b)), the measured walk-off gradually reduced for increasing frequency (Fig. 3(c)), given that the forcing term in Equation (1) reduces and φ_0 moves toward zero, corresponding to a null walk-off angle according to Equation (2). The crossover value was found to be $f_c = 15$ kHz (compatible with the values reported in literature $f_c \in [10\ \ 20]$ kHz, the latter strongly dependent on the temperature [34]), where the beam trajectory is nearly parallel to the z-direction, i.e., $\delta = 0^\circ$ (Fig. 3(d)). Noteworthy, as the nonlinear coefficient n_2 becomes lower (see Eqs. (1) and (4)), the optical reorientation is lower and the beam loses its self-trapped nature and diffracts. For frequencies higher than f_c, the absolute value of φ_0 begins to grow up: light undergoes self-confinement (n_2 does not depend on the sign of φ_0) and the beam steers toward negative angles (Fig. 3(e)) until saturation takes place at $\delta = -6.5^\circ$ (Fig. 3(f)). Thus, the overall spanned angle reaches 13°, which represents the maximum available beam steering ascribable solely to changes in walk-off via director rotation.

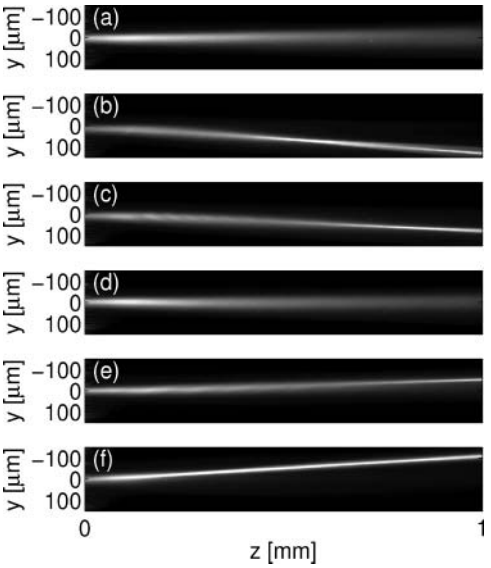

Figure 3. Acquired pictures of the beam evolution for different frequencies. (a) $V = 0$ V and the beam propagates in the linear regime, its trajectory being parallel to the z axis. (b–c) $V = 6$ V (like in the following panels) and $f = 1$–10 kHz: the beam is self-confined and propagates at positive walk-off angles (from $\delta = 6.5^\circ$), depending on the direction of the optic axis. (d) $f = f_c = 15$ kHz: the electric torque is null and the beam propagates as no voltage is applied. (e–f) $f = 20$–30 kHz: the dielectric anisotropy changes sign, as well as the walk-off, reaching $\delta = -6.5^\circ$ for $f = 30$ kHz.

Figure 4 shows the beam walk-off and width versus frequency f for three values of the amplitude V. Each walk-off curve follows the same qualitative behavior, crossing zero at $f_c = 15$ kHz. Moreover, the beam width normalized to w_0 for three voltage amplitudes

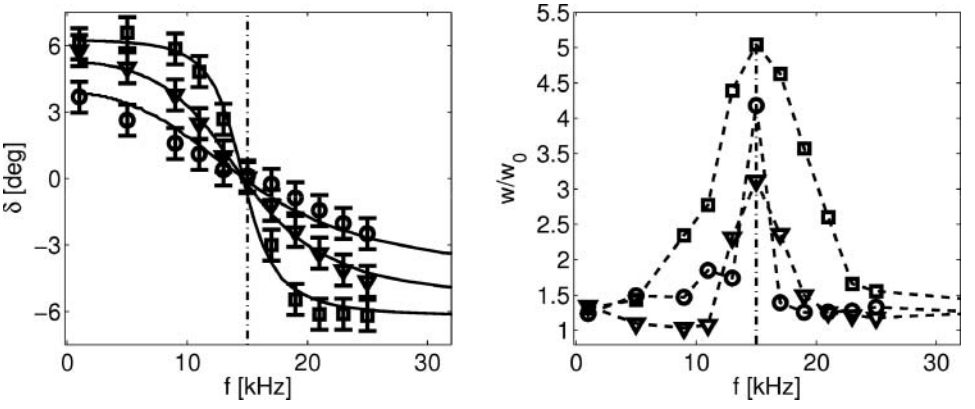

Figure 4. Measured walk-off (left panel) and normalized width (right panel) versus frequency, for voltage $V = 2.5$ V (circles), 3.5 V (triangles), and 6 V (squares). Solid line in the walk-off panel are calculated from Equation (3), while dashed lines in the width panel are guidelines for eyes. The vertical lines indicate the value of the crossover frequency at 15 kHz.

Downloaded by [Renmin University of China] at 11:06 13 October 2013

reveals the rapidly decrease of the nonlinearity in proximity of the crossover frequency, corroborating our theoretical model.

4. Conclusions

We reported about the control of nematicons properties in dual-frequency nematic liquid crystals. Employing a planar cell with suitable patterned electrodes, we induced planar reorientation of the molecular director, with saturation position parallel or perpendicular to the low-frequency applied field whether its frequency is lower or higher of the crossover value, respectively. We demonstrated how both the frequency and the amplitude of the applied bias affect the optical properties of the medium, focusing on the measurements of width and trajectory for self-confined waves. The studied configuration allows the maximization of the angular routing of nematicons based solely upon walk-off modulation: for a given optical anisotropy, overall deflection angle is twice the maximum of the walk-off angle.

Downloaded by [Renmin University of China] at 11:06 13 October 2013

References

[1] Yang, D. K., & Wu, S. T. (2006). *Fundamentals of Liquid Crystals Devices*, Wiley: New York.
[2] Khoo, I. C. (1995). *Liquid Crystals: Physical Properties and Nonlinear Optical Phenomena*, Wiley: New York.
[3] DeGennes, P. G., & Prost, J. (1993). *The Physics of Liquid Crystals*, Oxford Science: New York.
[4] Kivshar, Y. S., & Agrawal, G. P. (2003). *Optical Solitons*, Academic Press: San Diego, CA.
[5] Conti, C., & Assanto, G. (2004). In: *Encyclopedia of Modern Optics*, Vol. 5, Elsevier: Oxford, pp. 43–55.
[6] Suter, D., & Blasberg, T. (1993). *Phys. Rev. A 48*, 4583–4587.
[7] Conti, C., Peccianti, M., & Assanto, G. (2003). *Phys. Rev. Lett.*, *91*, 073901.
[8] Dauxois, T., & Peyrard, M. (2006). *Physics of Solitons*, Cambridge University Press: Cambridge.
[9] Boardman, A. D., & Sukhorukov, A. P. (Eds.). (2001). *Soliton-Driven Photonics*, Kluwer Academic: New York.
[10] Bjorkholm, J. E., & Ashkin, A. A. (1974). *Phys. Rev. Lett.*, *32*, 129–132.
[11] Duree, G. C., Shultz, J. L., Salamo, G. J., Segev, M., Yariv, A., Crosignani, B., Di Porto, P., Sharp, E. J., & Neurgaonkar, R. R. (1993). *Phys. Rev. Lett.*, *71*, 533–536.
[12] Torruellas, W. E., Assanto, G., Lawrence, B. L., Fuerst, R. A., & Stegeman, G. I. (1996). *Appl. Phys. Lett.*, *68*, 1449–1451.
[13] Rotschild, C., Cohen, O., Manela, O., Segev, M., & Carmon, T. (2005). *Phys. Rev. Lett.*, *95*, 213904.
[14] Khoo, I. C. (2009). *Phys. Rep.*, *471*, 221.
[15] Peccianti, M., & Assanto, G. (2012). *Phys. Rep.*, *516*, 147–208.
[16] Pasquazi, A., Alberucci, A., Peccianti, M., & Assanto, G. (2005). *Appl. Phys. Lett.*, *87*, 261104.
[17] Serak, S. V., Tabiryan, N. V., Peccianti, M., & Assanto, G. (2006). *IEEE Photon. Techn. Lett.*, *18*(12), 1287–1289.
[18] Piccardi, A., Bortolozzo, U., Residori, S., & Assanto, G. (2009). *Opt. Lett.*, *34*, 737.
[19] Peccianti, M., Assanto, G., Dyadyusha, A., & Kaczmarek, M. (2006). *Nat. Phys.*, *2*, 737.
[20] Peccianti, M., Conti, C., Assanto, G., De Luca, A., & Umeton, C. (2004). *Nature*, *432*, 733.
[21] Piccardi, A., Alberucci, A., & Assanto, G. (2010). *Appl. Phys. Lett.*, *96*, 061105.
[22] Piccardi, A., Alberucci, A., & Assanto, G. (2010). *Phys. Rev. Lett.*, *104*, 213904.
[23] Jeu, W. H., Gerritsma, C. J., Zanten, P. V., & Goossens, W. J. A. (1972). *Phys. Lett.*, *39A*, 355.
[24] Xianyu, H., Wu, S.-T., & Lin, C.-L. (2009). *Liq. Cryst.*, *36*, 717.
[25] Mottram, N. J., & Brown, C. V. (2006). *Phys. Rev. E*, *74*, 031703.

[26] Schadt, M. (1982). *Mol. Cryst. Liq. Cryst.*, *89*, 77.
[27] Golovin, A. B., Shiyanovskii, S. V., & Lavrentovich, O. D. (2003). *Appl. Phys. Lett.*, *83*, 3864.
[28] Lu, Y.-Q., Liang, X., Wu, Y.-H., Du, F., & Wu, S.-T. (2004). *Appl. Phys. Lett.*, *85*, 3354.
[29] Kao, Y.-Y., & Chao, P. C.-P. (2011). *Sensors*, *11*, 5402.
[30] Piccardi, A., Peccianti, M., Assanto, G., Dyadyusha, A., & Kaczmarek, M. (2009). *Appl. Phys. Lett.*, *94*, 091106.
[31] Wen, C.-H., & Wu, S.-T. (2005). *Appl. Phys. Lett.*, *86*, 231104.
[32] Alberucci, A., & Assanto, G. (2007). *J. Opt. Soc. Am. B*, *24*, 2314.
[33] Alberucci, A., Piccardi, A., Peccianti, M., Kaczmarek, M., & Assanto, G. (2010). *Phys. Rev. A*, *82*, 023806.
[34] Yin, Y., Shiyanovskii, S. V., & Lavrentovich, O. D. (2007). *Phys. Rev. Lett.*, *98*, 097801.

Downloaded by [Renmin University of China] at 11:06 13 October 2013